Available online at www.sciencedirect.com
ScienceDirect
Chemical Physics Letters 444 (2007) 9–16
CHEMICAL PHYSICS LETTERS
www.elsevier.com/locate/cplett

A three-dimensional morphed potential of Ne–HCl including the ground state deuterated Σ bending vibration

Luis A. Rivera-Rivera, Blake A. McElmurry, Sergey P. Belov, Robert R. Lucchese, John W. Bevan *

Department of Chemistry, Texas A&M University, Building 3255, College Station, TX 77843-3255, USA

Received 27 April 2007; in final form 22 June 2007
Available online 30 June 2007

Abstract

The ground state submillimeter spectrum of the Σ bending vibrations of ^{20}Ne–D^{35}Cl and ^{20}Ne–D^{37}Cl have been recorded in a coaxially-configured supersonic jet and band origin frequencies determined at 259.1348291(22) and 258.0180035(22) GHz, respectively. The recorded data were analyzed and included with other available experimental data to generate a fully three-dimensional morphed potential energy surface for the Ne–HCl potential having $V_{min}(0°) = -90.2(37)$ cm^{-1}, $R_{min}(0°) = 3.45(1)$ Å, and $V_{min}(180°) = -74.8(30)$ cm^{-1}, $R_{min}(180°) = 3.13(1)$ Å with a barrier height of 46.7(41) cm^{-1}. This morphed potential energy surface is compared with previously generated *ab initio* and semi-empirical potentials for Ne–HCl.

1. Introduction

Van der Waals complexes such as Rg–HX (Rg = Ne, Ar, Kr; X = F, Cl, Br, I) have become prototypical systems for investigation of vibration-rotation-tunneling dynamics. Comprehensive investigations in such homologous series provide fundamental perspectives on the influence of different intermolecular forces, particularly polarization and dispersion forces [1–3].

Ne–HCl was first observed experimentally in supersonic expansions by Novick et al. [4]. Their results were consistent with almost free rotation of the HCl molecule within the complex. Barton et al. [5] subsequently investigated ground vibrational state microwave and radiofrequency Stark spectra for Ne–DCl and a partially resolved rotational spectrum of Ne–HCl was obtained by Prout [6]. Hutson and Howard [7] calculated an anisotropic potential energy surface (PES) for Ne–HCl and determined a small barrier to internal rotation in the complex with a PES having a global minimum at the linear Ne–HCl configuration and a secondary minimum at the Ne–ClH configuration. Lovejoy and Nesbitt [8] later obtained a near-infrared spectrum of jet-cooled Ne–HCl, reporting the HCl stretching fundamental and three combination bands including those of the van der Waals stretching and bending modes in the excited state. Subsequently, Hutson [9] calculated a two-dimensional (2-D) PES for Ne–HCl with HCl in its $v = 1$ state, by least-squares fitting to the near-infrared laser spectra. This surface was also characterized by a global minimum at the linear Ne–HCl geometry, and a secondary minimum at the Ne–ClH linear geometry. Schuder et al. [10] later observed the Ne–DCl complex in a slit jet supersonic expansion analyzing the mid-infrared absorption spectra for the DCl stretch fundamental and the DCl bending combination bands. The DCl component was also found to be a nearly free rotor from anomalous intensity patterns for Ne–DCl, in contrast to the more restricted librational motion of DCl in Ar–DCl.

Potentials based on ground state *ab initio* calculations are available for the complex [11,12]. Those potentials also indicated a global minimum Ne–HCl and a secondary minimum Ne–ClH. Recently, Jiang et al. [13] performed *ab initio* calculations at the CCSD(T)/aug-cc-pVTZ-332 level of

* Corresponding author. Fax: +1 979 8454719.
E-mail address: bevan@mail.chem.tamu.edu (J.W. Bevan).

0009-2614/$ - see front matter © 2007 Elsevier B.V. All rights reserved.
doi:10.1016/j.cplett.2007.06.120

theory and found the Ne–ClH linear geometry more stable than the Ne–HCl linear geometry contradicting previous studies. However, a further investigation by Cagide Fajín et al. [14] at the CCSD(T)/aug-cc-pV5Z-33211 level of theory attributed the results of Jiang et al. [13] to use of an inadequate basis set. This surface was characterized by two linear minima, the global minimum Ne–HCl, and the secondary minimum Ne–ClH with a difference in energy less than 3 cm^{-1}.

Up to the present, substantial differences exist between the available 2-D potentials of Ne–HCl. These discrepancies make the comparison between the potentials for $v = 0$ and $v = 1$ states of HCl difficult and unreliable. Furthermore, it has been claimed that high quality *ab initio* potentials are more reliable than the semi-empirical ones [14]. Consequently, in order to get more insight about the dependence of the potential on the HCl bond length r, a 3-D surface is indispensable.

3-D morphed potentials have been determined for the related Ar–HBr [15,16] and Kr–HBr [17] complexes and have been found to provide semi-empirical potentials with enhanced accuracy for characterization of these complexes. In this work, we will report further experimental data for the Σ bend in the ground state of Ne–DCl complex to augment other available experimental data. This combined data is used to morph a 3-D *ab initio* PES and provide parameters with statistical errors for comparison with previously determined semi-empirical and theoretically generated potentials for this complex.

2. Experimental section

A submillimeter-wave spectrometer with coaxial pulsed jet configuration was used to record the ground state Σ bending vibrations in $^{20}Ne–D^{35}Cl$ and $^{20}Ne–D^{37}Cl$. A detailed description of this frequency and phase stabilized backward wave oscillator (BWO) based spectrometer has been given elsewhere [18–20] so only a brief description of the experiment is given here. The source of the submillimeter-wave radiation was an Istok OB-30 backward wave oscillator tunable from approximately 220–385 GHz by applying a variable high voltage in the range of 1–3.7 kV. A General Valve Series-9 500 μm diameter orifice pulsed-nozzle was used at a reservoir pressure sustained at approximately 40 psig with a 2% HCl: 98% Ne mixture. The vacuum system consists of a Varian 400 M diffusion pump backed by a Leybold RUVAC WA-251 Roots blower and a 1398 Welch mechanical pump. A vacuum pressure of 10^{-6} Torr or less was maintained without load and $<10^{-4}$ Torr with load when the pulsed valve was operated at 15 Hz repetition rate and duration of ~1 ms.

3. Theoretical calculations

3.1. Ab initio calculations

A new *ab initio* PES was calculated as a starting point for the morphing procedure. The non-relativistic interaction energy of Ne–HCl complex was evaluated at CCSD(T) level of theory with aug-cc-pVTZ [21,22] basis sets using the MOLPRO 2006 electronic structure package [23]. A grid of 780 (R, θ, r) points was calculated for a HCl bond distance, r, varied using the 6 point grid 1.074552, 1.174552, 1.274552, 1.374552, 1.474552 and 1.574552 Å, the distance Ne–Cl, R, varied using a grid of 13 points 3.00, 3.30, 3.40, 3.50, 3.70, 3.80, 3.85, 3.90, 4.00, 4.50, 5.00, 5.50 and 6.00 Å, and 10 equally spaced points between 0 and 180° along the H–Cl–Ne angle, θ. Interaction energies were then corrected for the basis set superposition error (BSSE) using the counterpoise (CP) method of Boys and Bernardi [24].

The fully BSSE corrected 3-D PES was obtained using

$$V(R, \theta, r) = V^{\text{int}}(R, \theta, r) + V^{\text{HCl}}(r), \quad (1)$$

where $V^{\text{int}}(R, \theta, r)$ is the BSSE corrected interaction energy, and $V^{\text{HCl}}(r)$ the interatomic potential for the isolated HCl molecule. $V^{\text{HCl}}(r)$ was chosen to be a 1-D Morse potential [25] with the parameters [26,27] $2\beta = 2.232932$, $D = 42341.90\ cm^{-1}$, and $r_e = 1.274552$ Å.

Computed interaction energies were then fitted to an analytical form using a 3-D interpolation function based on the Hilbert space reproducing kernel (HSRK) of Ho and Rabitz [28]. The approach is similar to the method used in Ar–HBr [15,16] where smoothing has been removed for similar reasons and the switching range Δx set to zero.

3.2. Calculations of rovibrational energy levels

Rovibrational energy levels were computed using the variational method previously described [15,29–31]. The

Table 1
Rovibrational parameters for Ne–DCl

Isotopomer state	v_0 (MHz)	B (MHz)	D_J (kHz)	H_J (Hz)[c]	χ_{aa} (MHz)	$D\chi_{aa}$ (kHz)
$^{20}Ne–D^{35}Cl$ $(0,2^0,0)$	259134.8291(22)	2654.62663(62)	67.442(49)	−0.2270(14)	−30.9209(71)	15.01(45)
$^{20}Ne–D^{35}Cl$[a] $(0,0^0,0)$		2698.13461(68)	182.662(61)	−0.0221(22)	−13.2881(71)	−4.69(52)
$^{20}Ne–D^{37}Cl$ $(0,2^0,0)$	258018.0035(22)	2614.74179(69)	72.940(60)	−0.19823(19)	−24.3318(74)	11.68(59)
$^{20}Ne–D^{37}Cl$[b] $(0,0^0,0)$		2648.95138(77)	177.077(81)	−14.1(33)	−10.5235(78)	−3.75(76)

[a] Compare with B (MHz) = 2698.1373(12), D_J (kHz) = 183.07(10), χ_{aa}(MHz) = −13.28692(94) [5] and B (MHz) = 2698.1387(12) and D_J (kHz) = 183.11(39) [10].

[b] Compare with B (MHz) = 2648.9471(9), D_J (kHz) = 176.77(19), χ_{aa}(MHz) = −10.522(2) [5].

[c] L_J (Hz) terms not accurately determined.

H–Cl stretching motion was adiabatically separated from the bending and stretching motion of the complex. At each value of R and θ, the energy of the HCl (v_1) stretching state $E_{v_1}(R, \theta)$ was determined. This energy then became the potential for the determination of the bending and stretching motion of the complex. The intermolecular rovibrational wave function was computed using a space-fixed frame with the radial functions expanded in a distributed Gaussian basis set. 50 functions were evenly distributed from $R = 2.700$ Å to $R = 6.600$ Å while the angular basis set contained an expansion of the rotational wave function of the HCl monomer, using states up to $j_{max} = 14$. All possible end-over-end rotational states were included, consistent with the value of j_{max} and the value of the total

Table 2
Experimental data used in the fits and fitted values with the uncertainties used

Observable	$V_{ab\ initio}$	$V_{morphed}$	Experiment	References	σ_k
^{20}Ne–D^{35}Cl $\{E[(0,2^0,0)_0]–E[(0,0^0,0)_0]\}$/cm^{-1}	13.5409	8.4075	8.6438	This work	0.05
^{20}Ne–D^{37}Cl $\{E[(0,2^0,0)_0]–E[(0,0^0,0)_0]\}$/cm^{-1}	13.6544	8.4058	8.6066	This work	0.05
^{20}Ne–H^{35}Cl $\{E[(1,0^0,0)_0]–E[(0,0^0,0)_0]\}$/cm^{-1}	−0.1717	0.2927	0.3024	[8]	0.03
^{20}Ne–D^{35}Cl $\{E[(1,0^0,0)_0]–E[(0,0^0,0)_0]\}$/cm^{-1}	−0.2795	0.1373	0.3128	[10]	0.03
^{20}Ne–H^{35}Cl $\{E[(1,2^0,0)_0]–E[(1,0^0,0)_0]\}$/cm^{-1}	18.8635	15.7917	15.6845	[8]	0.05
^{20}Ne–D^{35}Cl $\{E[(1,2^0,0)_0]–E[(1,0^0,0)_0]\}$/cm^{-1}	13.5715	8.3020	8.2043	[10]	0.05
^{20}Ne–H^{35}Cl $\{E[(1,0^0,1)_0]–E[(1,0^0,0)_0]\}$/cm^{-1}	20.6451	20.8246	20.8549	[8]	0.05
^{20}Ne–H^{35}Cl $\{E[(1,1^{1f},0)_1]–E[(1,0^0,0)_1]\}$/cm^{-1}	25.1458	22.9452	22.5245	[8]	0.05
^{20}Ne–D^{35}Cl $\{E[(1,1^{1f},0)_1]–E[(1,0^0,0)_1]\}$/cm^{-1}	17.9232	13.5476	13.5748	[10]	0.05
^{20}Ne–H^{35}Cl $B[(0,0^0,0)_{1,0}]$/(0.01 cm^{-1})	8.193	9.105	9.111	[7]	0.003
^{20}Ne–D^{35}Cl $B[(0,0^0,0)_{1,0}]$/(0.01 cm^{-1})	8.103	9.006	9.000	[5]	0.003
^{20}Ne–D^{37}Cl $B[(0,0^0,0)_{1,0}]$/(0.01 cm^{-1})	7.958	8.836	8.836	[5]	0.003
^{20}Ne–D^{35}Cl $B[(0,2^0,0)_{1,0}]$/(0.01 cm^{-1})	7.830	8.845	8.855	This work	0.003
^{20}Ne–D^{37}Cl $B[(0,2^0,0)_{1,0}]$/(0.01 cm^{-1})	7.702	8.729	8.722	This work	0.003
^{20}Ne–H^{35}Cl $B[(1,0^0,0)_{1,0}]$/(0.01 cm^{-1})	8.146	9.053	9.057	[8]	0.003
^{20}Ne–D^{35}Cl $B[(1,0^0,0)_{1,0}]$/(0.01 cm^{-1})	8.060	8.957	8.949	[10]	0.003
^{20}Ne–H^{35}Cl $B[(1,1^{1f},0)_{2,1}]$/(0.01 cm^{-1})	8.152	9.097	9.091	[8]	0.003
^{20}Ne–D^{35}Cl $B[(1,1^{1f},0)_{2,1}]$/(0.01 cm^{-1})	8.099	9.038	9.040	[10]	0.003
^{20}Ne–H^{35}Cl D_J $[(0,0^0,0)_{2,1,0}]$/(1.0×10^{-7} cm^{-1})	36.90	70.02	69.05	[8]	4.0
^{20}Ne–D^{35}Cl D_J $[(0,0^0,0)_{2,1,0}]$/(1.0×10^{-7} cm^{-1})	28.71	66.19	61.07	[5]	4.0
^{20}Ne–D^{37}Cl D_J $[(0,0^0,0)_{2,1,0}]$/(1.0×10^{-7} cm^{-1})	27.38	63.43	58.96	[5]	4.0
^{20}Ne–D^{35}Cl D_J $[(0,2^0,0)_{2,1,0}]$/(1.0×10^{-7} cm^{-1})	21.745	42.428	22.496	This work	4.0
^{20}Ne–D^{37}Cl D_J $[(0,2^0,0)_{2,1,0}]$/(1.0×10^{-7} cm^{-1})	21.933	48.001	24.330	This work	4.0
^{20}Ne–H^{35}Cl D_J $[(1,0^0,0)_{2,1,0}]$/(1.0×10^{-7} cm^{-1})	36.35	69.57	70.41	[8]	4.0
^{20}Ne–D^{35}Cl D_J $[(1,0^0,0)_{2,1,0}]$/(1.0×10^{-7} cm^{-1})	28.0	65.4	66.0	[10]	4.0
^{20}Ne–H^{35}Cl D_J $[(1,1^{1f},0)_{3,2,1}]$/(1.0×10^{-7} cm^{-1})	50.17	75.97	66.88	[8]	4.0
^{20}Ne–D^{35}Cl D_J $[(1,1^{1f},0)_{3,2,1}]$/(1.0×10^{-7} cm^{-1})	47.0	73.8	66.5	[10]	4.0
^{20}Ne–H^{35}Cl $\langle P_1(\cos\theta)\rangle$ for $(0,0^0,0)_0$	0.403	0.189	0.200	[7]	0.03
^{20}Ne–D^{35}Cl $\langle P_1(\cos\theta)\rangle$ for $(0,0^0,0)_0$	0.671	0.344	0.422	[5]	0.03
^{20}Ne–D^{37}Cl $\langle P_1(\cos\theta)\rangle$ for $(0,0^0,0)_0$	0.674	0.358	0.424	[5]	0.03
^{20}Ne–H^{35}Cl $\langle P_2(\cos\theta)\rangle$ for $(0,0^0,0)_0$	0.1657	0.0850	0.0812	[7]	0.004
^{20}Ne–D^{35}Cl $\langle P_2(\cos\theta)\rangle$ for $(0,0^0,0)_0$	0.37001	0.17482	0.19715	[5]	0.004
^{20}Ne–D^{37}Cl $\langle P_2(\cos\theta)\rangle$ for $(0,0^0,0)_0$	0.3736	0.1809	0.1983	[5]	0.004
^{20}Ne–D^{35}Cl $\langle P_2(\cos\theta)\rangle$ for $(0,2^0,0)_0$	0.2641	0.4172	0.4588	This work	0.004
^{20}Ne–D^{37}Cl $\langle P_2(\cos\theta)\rangle$ for $(0,2^0,0)_0$	0.2612	0.4145	0.4585	This work	0.004
^{20}Ne–D^{35}Cl$D_\theta^{(1,0)}/10^{-6}$for$(0, 0^0, 0)$	17.4	76.4	73.0	[5]	4.0
G	161.09	3.94			

Table 3
Optimized morphing parameters $C_{\alpha,i,j}$ and their corresponding uncertainties

(α,i,j)	$C_{\alpha,i,j}$	$C^0_{\alpha,i,j}$	σ
(1,0,0)	1.5339	1.0	0.0060
(1,0,1)	−1.261	0.0	0.035
(2,0,0)	(1.0)	1.0	Constrained
(2,1,0)	0.1767	0.0	0.0014
(2,2,0)	0.1314	0.0	0.0027
(3,0,0)	0.089283	0.0	0.000094
(3,1,0)	0.01953	0.0	0.00028
(3,2,0)	0.02215	0.0	0.00059

Table 4
Correlation matrix of the morphing parameters ($C_{\alpha,i,j}$)

(α,i,j)	(1,0,0)	(1,0,1)	(2,1,0)	(2,2,0)	(3,0,0)	(3,1,0)	(3,2,0)
(1,0,0)	1.00						
(1,0,1)	−0.38	1.00					
(2,1,0)	0.37	−0.18	1.00				
(2,2,0)	0.29	−0.19	0.54	1.00			
(3,0,0)	−0.45	0.12	−0.07	0.47	1.00		
(3,1,0)	0.47	−0.09	0.47	−0.36	−0.66	1.00	
(3,2,0)	0.33	−0.12	0.34	0.88	0.26	−0.43	1.00

angular momentum of a given state and the rovibrational states were computed in two steps. Initially, a vibrational self-consistent field (VSCF) calculation was performed in which the angular state was computed in an angular poten-

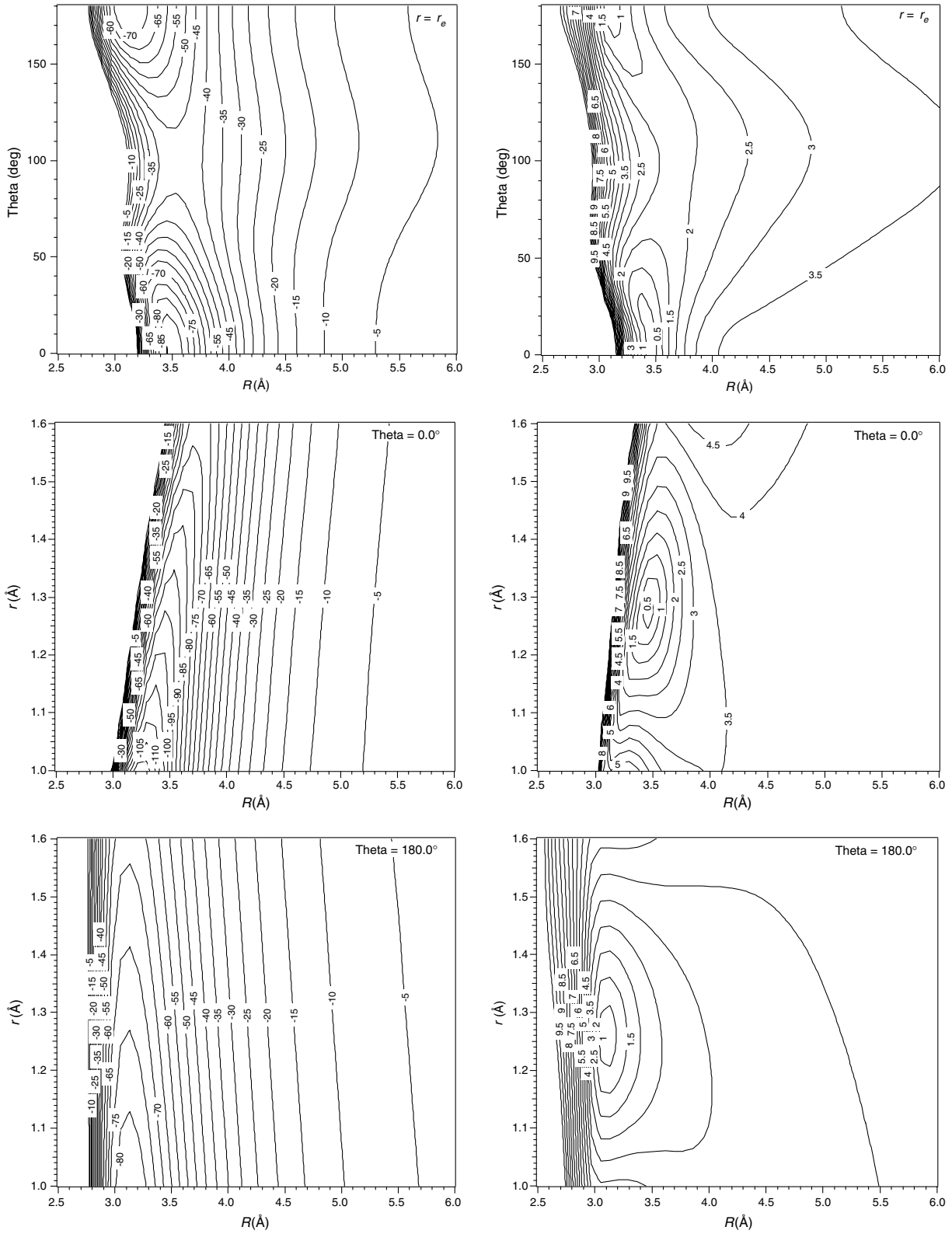

Fig. 1. Morphed interaction potential of Ne–HCl. Left panels give three cuts: $V^{\mathrm{int}}(R,\theta,r=r_{\mathrm{e}})$, $V^{\mathrm{int}}(R,\theta=0°,r)$ and $V^{\mathrm{int}}(R,\theta=180°,r)$. Panels on the right-hand side are the corresponding statistical uncertainties relative to the minimum of the potential, which occurs at $\theta=0.0°$, $R=3.45(1)$ Å, and $r=r_{\mathrm{e}}$, with $V_{\mathrm{min}}=-90.2(37)\,\mathrm{cm}^{-1}$. All contours are given in cm^{-1}. The coordinates used (R,θ,r) are Jacobi coordinates for the ^{20}Ne–H^{35}Cl isotopomer.

tial obtained from the full intermolecular potential by averaging over the ground radial vibrational state. The radial state was obtained from a 1-D vibrational calculation where the potential was determined from the full intermolecular potential by averaging over the bending state. The VSCF equations were solved iteratively. The converged VSCF bending and stretching wave functions were then combined in a direct product basis set, which was used in a vibrational configuration interaction (VCI) calculation for the final rovibrational states. Derivatives of the rovibrational eigenvalues with respect to the morphing parameters were computed using the Hellmann–Feynman theorem. The rotational constants used in the Hamiltonian for the diatomic fragments were taken to be the same as for the isolated molecules: 10.4401992 cm^{-1} [32] for $H^{35}Cl$ ($v = 0$), 10.136228 cm^{-1} [26] for $H^{35}Cl$ ($v = 1$), 5.3922717 cm^{-1} [32] for $D^{35}Cl$ ($v = 0$), 5.27978 cm^{-1} [10] for $D^{35}Cl$ ($v = 1$), and 5.3764902 cm^{-1} [32] for $D^{37}Cl$ ($v = 0$).

3.3. Morphing the ab initio potential

The *ab initio* potential, $V_{ab\ initio}(R,\theta,r)$, was morphed using the transformation

$$V_{\text{morphed}}(R,\theta,r) = S_1(\theta,r)V_{ab\ initio}[S_2(\theta,r)(R-R_F) + (1+S_3(\theta,r))R_F,\theta,r], \quad (2)$$

where

$$S_\alpha(\theta,r) = \sum_{i,j} C_{\alpha,i,j}P_i(\cos\theta)\left[1-\exp\left(-\beta\frac{r-r_e}{r_e}\right)\right]^j. \quad (3)$$

The parameters $C_{\alpha,i,j}$ are the morphing parameters, and are dimensionless with R_F selected to be 3.70 Å and β chosen to be 1.0. Values of the morphing parameters were obtained by a regularized nonlinear least-squares optimization [15] and the quality of the fit of the experimental data characterized by the root-mean-square deviation from the experimental data

$$G(\gamma) = \left\{\frac{1}{M}\sum_{k=1}^{M}\left[\frac{O_k^{\text{expt}} - O_k^{\text{calc}}(C_{\alpha,i,j})}{\sigma_k}\right]^2\right\}^{1/2}. \quad (4)$$

The value of the regularization parameter used in the fitting was $\gamma = 10.0$ where $G(\gamma = \infty)$ is the deviation from the experimental data of the observables predicted from the *ab initio* potential (i.e. the unmorphed potential).

4. Results and discussion

Spectra of both ^{20}Ne–DCl isotopes were observed using a predicted spectrum extrapolated from previous experimental data [10]. Quadrupole resolved spectra were measured from 225 to 304 GHz for $P(6)$ to $R(8)$ transitions in both ^{35}Cl and ^{37}Cl isotopomers. Frequencies for 80 and 71 transitions were measured, respectively for inclusion in the JPL SPFIT program [33] using a linear molecule Hamiltonian with RMS standard deviations of 1.73 and 1.43 kHz. The fitted results are given in Table 1. Each fitted transition was averaged over two Doppler components

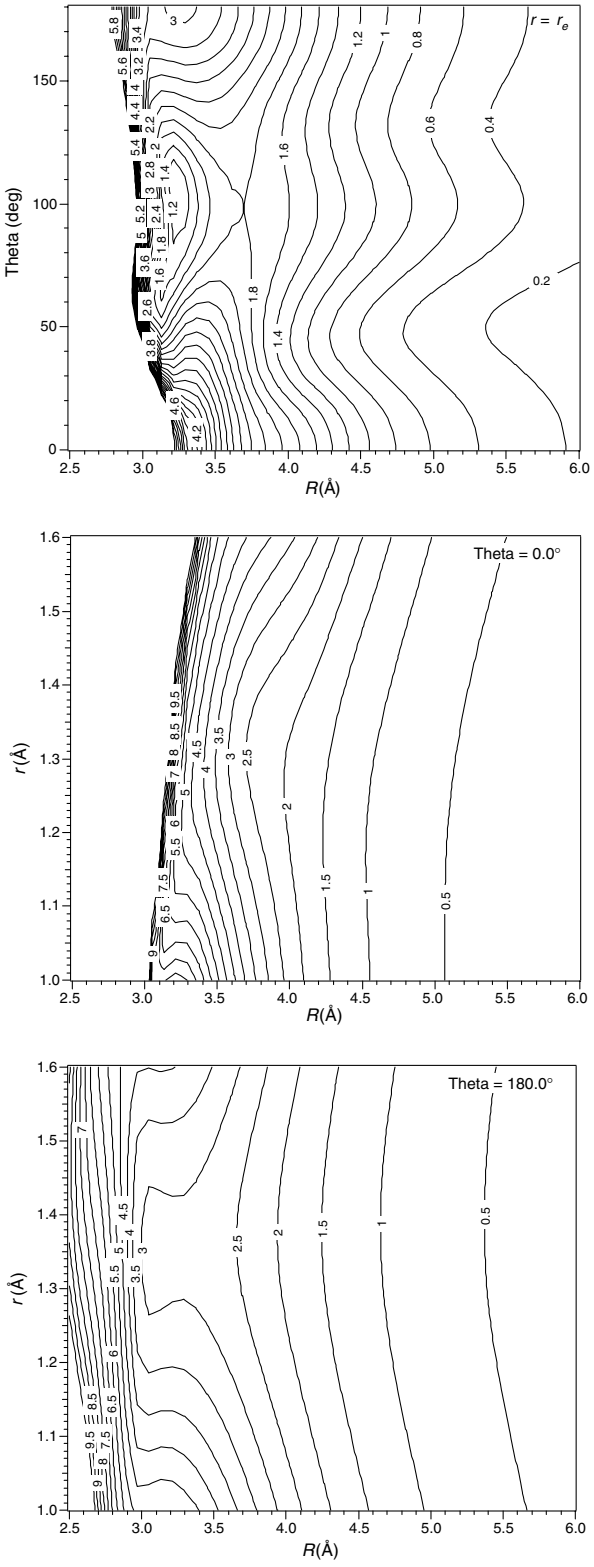

Fig. 2. Corresponding statistical uncertainties for the morphed interaction potential of Ne–HCl, relative to the value of the potential at infinite separation. All contours are given in cm^{-1}. The coordinates used (R,θ,r) are Jacobi coordinates for the ^{20}Ne–$H^{35}Cl$ isotopomer.

Table 5
Features of various Ne–HCl potentials

Parameter	$V_{ab\ initio}$[a]	$V_{morphed}$[a]	M4[b]	M5[b]	H6($v_1=1$)[b]	$V_{morphed}$[a] ($v_1=0$)	$V_{morphed}$[a] ($v_1=1$)	*ab initio*[c]	*ab initio*[d]
$V_{min}(0°)/cm^{-1}$	−58.58	−90.2(37)	−67.36	−68.22	−64.26	−81.4	−84.4	−58.99	−66.85
V_{min} (180°)/cm^{-1}	−48.49	−74.8(30)	−56.02	−53.50	−56.83	−57.5	−56.6	−61.55	−65.10
$V_{min}(0°)$–$V_{min}(180°)/cm^{-1}$	−10.09	−15.4(48)	−11.34	−14.72	−7.43	−23.9	−27.8	2.56	−1.75
Barrier height/cm^{-1}	30.38	46.7(41)	27.16	27.87	22.04	40.4	44.0	21.11	21.85
$R_{min}(0°)$/Å	3.91	3.45(1)	3.79	3.76	3.78	3.84	3.84	3.87	3.83
$R_{min}(180°)$/Å	3.45	3.13(1)	3.51	3.52	3.44	3.21	3.21	3.41	3.40
$R_{min}(0°)$–$R_{min}(180°)$/Å	0.46	0.32(2)	0.28	0.24	0.34	0.63	0.63	0.46	0.43

[a] This work.
[b] From [9].
[c] From [13]. CCSD(T)/aug-cc-pVTZ-332 level of theory.
[d] From [14]. CCSD(T)/aug-cc-pV5Z-33211 level of theory.

recorded by co-addition of 900 fast scan pulse signals [18–20]. The estimated accuracy of each center frequency is expected to be 1 kHz or better with the linewidth of 30 kHz observed for each quadrupole component so determined constants in both ground and excited state are expected to be evaluated with state-of-the-art microwave accuracy. Currently determined ground state rotational parameters can be compared with previous studies (Table 1) though additional H_j and χ_{jj} constants are included in our fits. The ground state v_0 band origin frequencies have been determined with estimated absolute accuracies of better than 1 kHz.

The experimental data used in the morphed PES of Ne–HCl is shown in Table 2. Such data included information obtained in the present study and also previously reported microwave and IR experiments [5,8,10]. Rotational constants and centrifugal distortion constants for the states $(1,2^0,0)$, $(1,0^0,1)$, and $(1,1^{1e},0)$ were not included in the fitting because such constants are significantly perturbed by Coriolis interactions. The values of G in Table 2 for the *ab initio* and morphed potentials are $G=161.09$ and $G=3.94$, respectively, indicating the improvement in the overall agreement with experiment obtained with the morphing procedure.

In Table 3, final morphing parameters are given that yielded the best fit of the experimental data. Since the morphing procedure is a nonlinear least-squares fit, there is always the possibility of other similar or better fits. The correlation matrix for the final morphing parameters is given in Table 4.

The morphed interaction PES of Ne–HCl is shown in Fig. 1 in the left panels, and the corresponding statistical uncertainties relative to the minimum of the potential are given in right panels. In addition, the statistical uncertainties relative to the value of the potential at infinite separation are given in Fig. 2. Plots are presented in Jacobi coordinates where R is the distance from ^{20}Ne to the center of mass of H^{35}Cl, θ is the angle ^{20}Ne-(center of mass of H^{35}Cl)–H. When $\theta=0°$ it corresponds to the Ne–H–Cl structure, and when $\theta=180°$ to the Ne–Cl–H structure. The morphed potential is characterized by two linear minima, the Ne–H–Cl minimum having $R_{min}=3.45(1)$ Å corresponding to $V_{min}=-90.2(37)$ cm^{-1} and the Ne–Cl–H minimum with $R_{min}=3.13(1)$ Å and $V_{min}=-74.8(30)$ cm^{-1}.

In Tables 5 and 6, the generated 3-D morphed potential has been compared with other available potentials for Ne–HCl. The 3-D morphed potential is found to give significantly deeper minima that the corresponding parameters in other determined potentials. Furthermore, the values of $R_{min}(0°)$ and $R_{min}(180°)$ are significantly smaller for the 3-D morphed potential. However, D_0, the dissociation energy is determined to be in the same range of previous calculated values [7,9,10,13,14] (Table 6). In addition, the energy difference between the two minima in the 3-D morphed potential of 15.4(48) cm^{-1}, compares with 14.72 cm^{-1} obtained form the M5 potential [9], but significantly larger than the value determined from the H6($v_1=1$) potential (Table 5). Lastly, the barrier height for the internal rotation of HCl subunit was determined to be 46.7(41) cm^{-1}, which is considerably larger than the previously determined values [9,13,14] (Table 5).

Additional experimental data for Ne–H(D)Cl with H(D)Cl in its $v=0$ state, especially D_0, will be necessary

Table 6
Comparison of D_0 values for Ne–HCl

	D_0 (cm^{-1})	References
^{20}Ne–H^{35}Cl($v_1=0$)	−30.115	This work (*ab initio*)
	−34.719	This work (morphed)
	−35.706	M4 [7]
	−35.095	M5 [7]
	−35.068	H6($v_1=1$) [9]
	−33.848	*ab initio* [13]
	−36.225	*ab initio* [14]
^{20}Ne–D^{35}Cl($v_1=0$)	−33.022	This work (*ab initio*)
	−35.257	This work (morphed)
	−36.058	H6($v_1=1$) [10]
	−34.498	*ab initio* [13]
^{20}Ne–H^{35}Cl($v_1=1$)	−30.286	This work (*ab initio*)
	−34.426	This work (morphed)
	−35.093	H6($v_1=1$) [9]
^{20}Ne–D^{35}Cl($v_1=1$)	−33.301	This work (*ab initio*)
	−35.120	This work (morphed)
	−36.094	H6($v_1=1$) [9]

Table 7
Comparison of predicted and observed $^{20}Ne–H^{35}Cl$ and $^{20}Ne–D^{35}Cl$ vibrational frequencies (cm^{-1})

Vibration	Σ bend $(v_1, 2^0, 0)$	vdW stretch $(v_1, 0^0, 1)$	Π bend $(v_1, 1^{1f}, 0)$
$^{20}Ne–H^{35}Cl$ ($v_1 = 0$)			
Calculated, *ab initio*[a]	19.2931	20.6142	25.7375
Calculated, Morphed[a]	16.3493	20.8083	23.3654
Calculated, M4 [7]	16.681	20.026	23.733
Calculated, M5 [7]	16.940	19.729	23.596
Calculated, H6($v_1 = 1$) [9]	16.080	21.006	23.354
Calculated, *ab initio* [13]	16.663	19.962	23.242
Calculated, *ab initio* [14]	16.768	20.226	23.749
$^{20}Ne–H^{35}Cl$ ($v_1 = 1$)			
Observed [8]	15.6845	20.8549	22.5245
Calculated, *ab initio*[a]	18.8635	20.6451	25.1458
Calculated, Morphed[a]	15.7917	20.8246	22.9452
Calculated, H6($v_1 = 1$) [9]	15.686	20.858	22.764
Calculated, *ab initio* [13]	16.171	19.608	22.359
$^{20}Ne–D^{35}Cl$ ($v_1 = 0$)			
Observed[a]	8.6438		
Calculated, *ab initio*[a]	13.5409	22.8286	18.0177
Calculated, Morphed[a]	8.4075	19.8023	13.5903
Calculated, *ab initio* [13]	8.323	18.784	
Calculated, H6($v_1 = 1$) [10]	8.393	20.217	13.675
$^{20}Ne–D^{35}Cl$ ($v_1 = 1$)			
Observed [10]	8.2043		13.5748
Calculated, *ab initio*[a]	13.5715	23.0099	17.9232
Calculated, Morphed[a]	8.3020	19.9229	13.5476
Calculated, H6($v_1 = 1$) [10]	8.219	20.232	13.476

[a] This work.

in order to determined an accurate potential well depth, D_e. The fact that the D_0 does not change with a deeper morphed potential can be attributed to the fact that the morphed potential has a bigger barrier for the internal rotation of HCl subunit. Since the wave functions for the states considered here are delocalized corresponding to nearly free rotor states, the net shift of the rovibrational energy levels upon morphing results from the near cancellation of the positive shift in the energies due to the increase in the barrier height and a negative shift in the energies due to deeper minima.

The morphed potentials in the $v = 0$ and $v = 1$ states of HCl in columns seven and eight in Table 5 provide a more relevant comparison with the M4, M5 and H6($v_1 = 1$) potentials, respectively. The well depth for the morphed potentials in the $v = 0$ and $v = 1$ states are deeper in the Ne–HCl configuration but, substantially the same in the Ne–ClH configuration, in comparison to the M4, M5, and H6($v_1 = 1$) potentials. In addition, the barrier height is larger for the morphed potentials in the $v = 0$ and $v = 1$ states than for the M4, M5 and H6($v_1 = 1$) potentials. Furthermore, the values of $R_{min}(0°)$ and $R_{min}(180°)$ for the morphed potentials in the $v = 0$ and $v = 1$ states are significantly different that the values determined for the M4, M5 and H6($v_1 = 1$) potentials.

In Table 7, the experimentally observed vibrational frequency of various states of $^{20}Ne–H^{35}Cl$ and $^{20}Ne–D^{35}Cl$ have been compared with theoretical predictions and found to be in the same range as calculated values [7–10,13,14]. Furthermore, in Table 8, predictions from the morphed potential have been given for some as yet unobserved transitions in $^{20}Ne–H^{35}Cl$ and $^{20}Ne–D^{35}Cl$.

5. Conclusions

The submillimeter Σ bending vibrations of $^{20}Ne–D^{35}Cl$ and $^{20}Ne–D^{37}Cl$ have been recorded using a coaxially configured submillimeter jet spectrometer and the band origins have been determined to be at 259.134891(22) and 258.0180035(22) GHz, respectively. The data obtained from these analyses have been combined with previously recorded microwave, radio frequency and infrared data and used to evaluate a vibrationally 3-D morphed potential for the complex. The morphed potential is consistent with a double minimum potential with $V_{min}(0°) = -90.2(37)\ cm^{-1}$, $R_{min}(0°) = 3.45(1)$ Å, and $V_{min}(180°) = -74.8(30)\ cm^{-1}$, $R_{min}(180°) = 3.13(1)$ Å with a barrier of $46.7(41)\ cm^{-1}$. From the present analysis, we conclude that the global and local minima in Ne–HCl have significantly deeper minima, a larger barrier, and smaller $R_{min}(0°)$ and $R_{min}(180°)$ than determined in previous potentials. Comparable trends have been determined from the extensive morphing studies of the Ar–HBr complex [15,16]. This is

Table 8
Predicted spectroscopic constants from the morphed potential for Ne–HCl

Isotopomer	State	B ($\times 10^{-2}\ cm^{-1}$)	D_J ($\times 10^{-7}\ cm^{-1}$)	$\langle P_1(\cos\theta)\rangle$	$\langle P_2(\cos\theta)\rangle$
$^{20}Ne–H^{35}Cl$	$(0, 2^0, 0)$	9.326	95.17	−0.1592	0.3424
$^{20}Ne–H^{35}Cl$	$(0, 0^0, 1)$	7.364	−78.71	−0.0294	0.0929
$^{20}Ne–H^{35}Cl$	$(0, 1^{1f}, 0)$	9.116	75.25	0.0337	−0.1832
$^{20}Ne–D^{35}Cl$	$(0, 0^0, 1)$	7.951	181.14	−0.1725	0.0698
$^{20}Ne–D^{35}Cl$	$(0, 1^{1f}, 0)$	9.051	73.44	0.0593	−0.1658
$^{20}Ne–D^{35}Cl$	$(1, 0^0, 1)$	7.923	184.67	−0.1775	0.0710

in contrast to corresponding morphed potentials determined for Ne–HBr [3] and particularly Ne–IH [34] which give convincing evidence for the existence of Ne–XH global minima in cases where polarization interactions are expected to be smaller and dispersion effects larger thus favoring van der Waals global minima.

Acknowledgement

We gratefully acknowledge the financial support of the National Science Foundation through Grants DMS-0216275 and CHE-0613202 and the Robert A. Welch Foundation (Grant A747).

References

[1] J.M. Hutson, Annu. Rev. Phys. Chem. 41 (1990) 123.
[2] R.C. Cohen, R.J. Saykally, J. Phys. Chem. 96 (1992) 1024.
[3] R.R. Lucchese, J.W. Bevan, F.J. Lovas, Chem. Phys. Lett. 398 (2004) 544.
[4] S.E. Novick, P.B. Davies, T.R. Dyke, W. Klemperer, J. Am. Chem. Soc. 95 (1973) 8547.
[5] A.E. Barton, D.J.B. Howlett, B.J. Howard, Mol. Phys. 41 (1980) 619.
[6] J.M. Prout, BA Thesis, Part II, Oxford University (1981).
[7] J.M. Hutson, B.J. Howard, Mol. Phys. 45 (1982) 769.
[8] C.M. Lovejoy, D.J. Nesbitt, Chem. Phys. Lett. 147 (1988) 490.
[9] J.M. Hutson, J. Chem. Phys. 91 (1989) 4448.
[10] M.D. Schuder, D.D. Nelson Jr., D.J. Nesbitt, J. Chem. Phys. 94 (1991) 5796.
[11] V. Subramanian, D. Sivanesan, T. Ramasami, Chem. Phys. Lett. 295 (1998) 312.
[12] T.J. Dudley, R.R. Pandey, P.E. Staffin, M.R. Hoffmann, G.C. Schatz, J. Chem. Phys. 114 (2001) 6166.
[13] L. Jiang, Z. Hua, X. Dai-Qian, Y. Guo-Sen, Chem. J. Chinese Univ. 24 (2003) 686.
[14] J.L. Cagide Fajín, J. López Cacheiro, B. Fernández, J. Chem. Phys. 121 (2004) 4599.
[15] J. Castillo-Chará, R.R. Lucchese, J.W. Bevan, J. Chem. Phys. 115 (2001) 899.
[16] Z. Wang, A.L. McIntosh, B.A. McElmurry, J.R. Walton, R.R. Lucchese, J.W. Bevan, J. Phys. Chem. A 109 (2005) 8168.
[17] Z. Wang, R.R. Lucchese, J.W. Bevan, J. Phys. Chem. A 108 (2004) 2884.
[18] B.A. McElmurry, R.R. Lucchese, J.W. Bevan, S.P. Belov, Phys. Chem. Chem. Phys. 6 (2004) 5318.
[19] B.A. McElmurry, R.R. Lucchese, J.W. Bevan, I.I. Leonov, S.P. Belov, A.C. Legon, J. Chem. Phys. 119 (2003) 10687.
[20] S.P. Belov, B.A. McElmurry, R.R. Lucchese, J.W. Bevan, I. Leonov, Chem. Phys. Lett. 370 (2003) 528.
[21] T.H. Dunning Jr., J. Chem. Phys. 90 (1989) 1007.
[22] D.E. Woon, T.H. Dunning Jr., J. Chem. Phys. 98 (1993) 1358.
[23] H.-J. Werner et al., MOLPRO, Version 2006. 1, A package of *ab initio* programs, Cardiff, UK, 2006.
[24] S.F. Boys, F. Bernardi, Mol. Phys. 19 (1970) 553.
[25] H.M. Hulburt, J.O. Hirschfelder, J. Chem. Phys. 9 (1941) 61.
[26] D.H. Rank, B.S. Rao, T.A. Wiggins, J. Mol. Spectrosc. 17 (1965) 122.
[27] K.P. Huber, G. Herzberg, Molecular Spectra and Molecular Structure IV. Constants of Diatomic Molecules, van Nostrand Reinhold Co, New York, 1979.
[28] T.-S. Ho, H. Rabitz, J. Chem. Phys. 104 (1996) 2584.
[29] A. Quiñones, G. Bandarage, J.W. Bevan, R.R. Lucchese, J. Chem. Phys. 97 (1992) 2209.
[30] A. McIntosh, A.M. Gallegos, R.R. Lucchese, J.W. Bevan, J. Chem. Phys. 107 (1997) 8327.
[31] J. Han, A.L. McIntosh, Z. Wang, R.R. Lucchese, J.W. Bevan, Chem. Phys. Lett. 265 (1997) 209.
[32] F.C. De Lucia, P. Helminger, W. Gordy, Phys. Rev. A 3 (1971) 1849.
[33] H.M. Pickett, J. Mol. Spectrosc. 148 (1991) 371.
[34] P. Lin, W. Jabs, R.R. Lucchese, J.W. Bevan, D.J. Brugh, R.D. Suenram, Chem. Phys. Lett. 356 (2002) 101.